





Exploiting a strong coupling regime of organic pentamer surface plasmon resonance based on the Otto configuration for creatinine detection

MUHAMMAD ASIF AHMAD KHUSHAINI,¹ NUR HIDAYAH AZEMAN,²
MUHAMAD MAT SALLEH,¹ TG HASNAN TG ABDUL AZIZ,^{1,4} AHMAD
ASHRIF A BAKAR,²  RICHARD M. DE LA RUE,³ AND AHMAD RIFQI
MD ZAIN^{1,5} 

¹Institute of Microengineering and Nanoelectronics, Universiti Kebangsaan Malaysia, 43600 UKM Bangi, Selangor, Malaysia

²Department of Electrical, Electronic and Systems Engineering, Faculty of Engineering and Built Environment, Universiti Kebangsaan Malaysia, 43600 UKM Bangi, Selangor, Malaysia

³School of Engineering, Rankine Building, University of Glasgow, Glasgow G12 8LT, United Kingdom

⁴hasnan@ukm.edu.my

⁵rifqi@ukm.edu.my

Abstract: The sandwiched material-analyte layer in the surface plasmon resonance (SPR)-Otto configuration emulates an optical cavity and, coupled with large optical nonlinearity material, the rate of light escaping from the system is reduced, allowing the formation of a strong coupling regime. Here, we report an organic pentamer SPR sensor using the Otto configuration to induce a strong coupling regime for creatinine detection. Prior to that, the SPR sensor chip was modified with an organic pentamer, 1,4-bis[2-(5-thiophene-2-yl)-1-benzothiophene]-2,5-dioctyloxybenzene (BOBzBT₂). To improve the experimental calibration curve, a normalisation approach based on the strong coupling-induced second dip was also developed. By using this procedure, the performance of the sensor improved to 0.11 mg/dL and 0.36 mg/dL for the detection and quantification limits, respectively.

© 2022 Optica Publishing Group under the terms of the [Optica Open Access Publishing Agreement](#)

1. Introduction

A chronic kidney disease (CKD) is defined as a gradual loss of kidney function and can be diagnosed by monitoring the pathophysiological level of the biomolecule creatinine [1]. Creatinine is produced by creatinine phosphate breakdown and is normally excreted by the kidneys. Depending on the lifestyle of a person, the normal level of creatinine in the serum is between 0.6 and 1.2 mg/dL [2]. The current approach for determining creatinine levels is Jaffe calorimetry. There are two phases to this procedure. The first step is to take blood samples and mix them with potassium oxalate before diluting them with purified water. Before filtering, sodium tungstate and 67 percent sulfuric acid are added to create a colourless, protein-free filtrate (PFF) solution. The PFF solution was then mixed with picric acid in the alkaline solution, causing an increase in light absorption at 500 nm due to the interaction with the creatinine molecules [3]. However, interference with other metabolites, as well as the time-consuming and limited accuracy of Jaffe's colorimetry, sparked interest in other alternative techniques [4].

A Surface plasmon resonance (SPR) can be induced by coupling the evanescent wave produced by total internal reflection with the collective oscillation of electrons at a metallic surface. This coupling action enables wavevector matching between the incident light and the surface plasmon [5]. At a given angle and wavelength, the resonance condition is fulfilled, leading in a considerable attenuation of reflectivity. When the local refractive index (RI) near the metallic surface changes, the aforementioned resonance condition changes and can be utilized

for a number of sensing applications [6,7]. The standard configuration uses a metallic thin film functionalized with a variety of sensing materials. The interaction between the analyte of interest and the sensing material alters the RI and results in a resonance shift [8]. Medical diagnostics [9], environmental monitoring [10], biochemistry [11], and food safety [12] have all seen widespread usage of sensors that employ the SPR principle. These sensors commonly utilize varying angle of incidence approaches to measure RIs, however they frequently have limited sensitivity [13].

Owing to its practicality, many SPR-based sensors were developed based on the Kretschmann configuration [14]. In this configuration, a sensor chip, which is usually made of a metallic thin film, deposited on the substrate slide is placed on top of the coupling prism [15,16]. However, to ensure that the discrepancy between the RI of the prism and the slide is eliminated, the selection of an index matching gel or fluid is crucial [17]. Another less common approach is the Otto configuration, which takes advantage of frustrated total internal reflection by coupling the tail of an evanescent wave at a prism/dielectric interface and the surface plasmon (SP) at the dielectric/metal interface [18]. Due to the placement of the dielectric or the analyte of interest in-between the prism and the metal layer, the need for index matching gel or fluid is eliminated [19].

The Otto-based SPR sensor has recently attracted a lot of attention [20–23]. This is owing to the fact that with the Otto configuration, considerably thicker metallic films can be employed compared to the 100 nm thickness constraint in the Kretschmann configuration, which minimizes optical losses [24]. In addition, the sandwiched structure creates an optical cavity, which increases the coupling efficiency between the SP and the material excitons [25–27]. As a result of the Rabi splitting process, the strong coupling regime is formed. In this regime, a hybrid mode with distinct characteristics compared to the original mode is formed [28,29]. This hybrid mode can be exploited for sensitivity enhancement in sensor applications [30–32]. The change in the degree of the interaction between a sensing material and a different concentration of the analyte could result in the formation of a distinct hybrid mode. This altered the splitting width, which may be correlated to analyte concentration to establish the sensor's calibration curve.

The present work reports the exploitation of the strong coupling in an organic pentamer-based SPR sensor that uses the Otto configuration for creatinine detection. The gold (Au) film SPR sensor chip was immobilized with different concentrations of an organic pentamer, 1,4-bis[2-(5-thiophene-2-yl)-1-benzothiophene]-2,5-dioctyloxybenzene (BOBzBT₂). Organic materials have attracted considerable attention in recent years due to their large dipole moments and high possible density [33]. Material with a large dipole moment is ideal for observing the strong coupling regime at room temperature because it increases the strength of the excitons-plasmon coupling [34]. The bis-donor groups in BOBzBT₂ enhance two-photon absorption efficiency, while the extended π -conjugated backbone of BOBzBT₂ elongates the charge-transfer network [35,36]. Subsequently, a normalization procedure that utilizing the strong coupling-induced dip is proposed to improve the experimental calibration curve.

2. Methods

2.1. Preparation of materials

The synthesis of the BOBzBT₂ (see Fig. 1(A)) was carried out via four transition compounds, namely: 1,4-bis(octyloxy)benzene (1); 2,5-dibromo-1,4-bis(octyloxy)benzene (2); 1,4-bis(thiophen-2-yl)-2,5-dioctyloxybenzene (3); and 1,4-bis(5-bromo-thiophen-2-yl)-2,5-dioctyloxybenzene (4) following the previous work in [37]. Williamson etherification and bromination reactions were used to prepare compound (1) and (2), respectively. Later, the Suzuki coupling reaction was carried out to synthesis compound (3) and compound (4) was prepared via bromination reaction. By replacing the thiophene boronic acid with benzo[b]thien-2-ylboronic acid for the latter Suzuki coupling reaction, the 1,4-bis[2-(5-thiophen-2-yl)-1-benzothiophene]-2,5-dioctyloxybenzene pentamer (BOBzBT₂) is prepared.

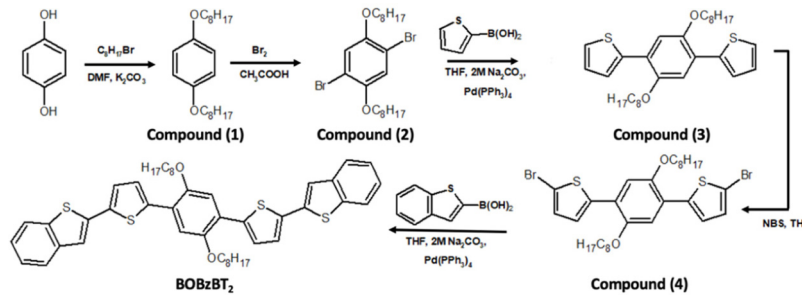


Fig. 1. The synthetic route of the BOBzBT₂ pentamer via transition compounds.

As a result of functionalization of dioctyloxy-substituents on phenylene moiety, BOBzBT₂ pentamer demonstrated good solubility producing a clear orange-coloured solution in common organic solvents such as chloroform (CHCl₃) with their respective maximum solubility limit of 6.31mg/mL. Additional thiophene moieties alongside the phenyl monomers increase optical nonlinearity of the pentamer [38]. Different concentrations of the BOBzBT₂ were prepared by diluting it with the CHCl₃ solvent. Three BOBzBT₂:CHCl₃ ratios (mg:ml) were prepared namely, 1BOBzBT₂: 3CHCl₃, 1BOBzBT₂: 2CHCl₃ and 3BOBzBT₂: 5CHCl₃. The creatinine solution (5 mg/dL) was prepared by dissolving 12.5 mg of creatinine with deionized water in a 250 ml (2.5 dL) volumetric flask. A series of different concentrations of creatinine dilutions were then prepared.

2.2. SPR-Otto configuration

The SPR sensor chip was fabricated by depositing a 50 nm Au layer on a 0.17 mm thick glass substrate using sputtering machine with 60 mA and 9 nm/min of sputtering current and rate, respectively. The BOBzBT₂ dilution was later immobilized on top of the film by spin-coating 1 mL of the BOBzBT₂:CHCl₃ dilution at 3,000 RPM for 40 s (Fig. 2(A)). A group of 10 sensor chips prepared for each BOBzBT₂:CHCl₃ dilution corresponding to nine different creatinine solution concentrations - and one blank solution. An SPR measurement based on the Otto configuration was prepared by first dropping creatinine solution on top of the prism before placing the bare Au or the BOBzBT₂:CHCl₃-Au sensor chips on top of the solution (see Fig. 2(B)).

In the Otto configuration, the damping of the system is contributed by the internal and radiative mechanisms. The former results from the absorption by the metallic film and has a proportional relationship with the complex dielectric constant. Meanwhile, radiative damping occurs due to the emission of the SP back into the prism. The coupling of this back wave strongly depends on the thickness of the spacer, i.e., the gap between the film and the prism [8]. Previously, several schemes for controlling the gap were proposed, such as using a pre-defined thickness spacer coating [39], a dielectric polymer spacing layer [40], or dual-resonance fibre [41].

In the present work, an iron block weighing 5 grams was placed on top of the sensor chip and left for 5 minutes (see Fig. 2(C)). This is to give the excess creatinine solution time to ooze out of the layer. Moreover, by applying a uniform and consistent load to the slide, a relatively uniform spacer thickness can be obtained. A DH-2000-BAL Ocean Optics unit supplied the broadband UV-VIS-NIR incident light. Light is incident through a polariser on the BK7 glass right-angle prism at an angle of incidence of $\theta = 18^\circ$, and its reflectance was collected by an HR2000CG-UV-NIR Series High-Resolution Fiber Optic Spectrometer.

At a critical angle, the total internal reflection induces an evanescent wave in the BOBzBT₂:CHCl₃-Creatinine layer as depicted in the inset of Fig. 2(C). Due to the presence of the evanescent wave, BOBzBT₂:CHCl₃-Creatinine excitons were created. The working principle behind this

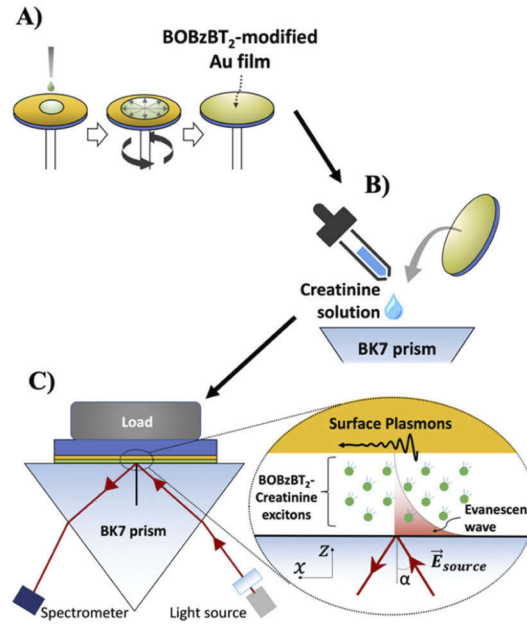


Fig. 2. A) The preparation of BOBzBT₂:CHCl₃ sensor chip, B) Preparation of SPR measurement on creatinine solutions, and, C) Schematic of an SPR setup using the Otto configuration. Inset show the interaction between excitons, SP and the evanescent wave.

is identical to that of total internal reflection (TIR) microscopy [42]. When the metallic film is brought into proximity to the prism, frustrated total internal reflection occurs and results in coupling between the associated evanescent wave, the BOBzBT₂:CHCl₃-Creatinine excitons and the SP mode. By varying the creatinine concentration, different SP-excitons couplings are generated. Through this principle, the concentration of an analyte can be quantified.

2.3. Theoretical background

The relation for the wave vector along the surface plasmon propagation can be expressed by:

$$k_x = \sqrt{\frac{\epsilon'_1 \epsilon_2}{\epsilon'_1 + \epsilon_2}} \frac{\omega}{c} + i \left(\frac{\epsilon'_1 \epsilon_2}{\epsilon'_1 + \epsilon_2} \right)^{1/2} \frac{\epsilon''_1 \epsilon_2}{2\epsilon'_1 (\epsilon'_1 + \epsilon_2)} \frac{\omega}{c} \quad (1)$$

where ϵ'_1 and ϵ''_1 are the real and imaginary term of dielectric function of the Au film. Meanwhile, ϵ_2 is the dielectric constant of BOBzBT₂:CHCl₃-Creatinine layer. To evaluate Eq. (1), the value of dielectric function for the Au is estimated by solving the Drude-Sommerfeld dynamical equation for a free-electron [43]:

$$\epsilon_1 = 1 - \frac{\omega_p^2}{\omega^2 + \gamma^2} + i \frac{\gamma \omega_p^2}{\omega(\omega^2 + \gamma^2)} \quad (2)$$

ω_p and γ are the bulk plasma frequency and the damping term for bulk gold, respectively. The Drude-Sommerfeld model gives accurate results in the infrared regime but is fails at wavelengths below 550 nm [44]. In the following analysis, the value $\omega_p = 13.8 \times 10^{15} \text{ s}^{-1}$ and $\gamma = 1.075 \times 10^{14} \text{ s}^{-1}$ were selected according to the Ref. [45]. These values were determined using [46] in the near-infrared region - and for a gold film thickness that exceeds the 25 nm thickness threshold.

Fresnel analysis at the boundary is then applied, with the tangential component of the electric field being continuous at both interfaces. The expression for the reflectance of a transverse magnetic wave is determined as follows [47]:

$$R = \left| \frac{r_{32} + r_{21} \exp(-2k_x d)}{1 + r_{32} r_{21} \exp(-2k_x d)} \right|^2 \quad (3)$$

where we have used the respective Fresnel reflection coefficients r_{32} and r_{21} for the BK7 - BOBzBT₂:CHCl₃-Creatinine layer (ϵ_3 and ϵ_2) and for the BOBzBT₂:CHCl₃-Creatinine layer - Au (ϵ_2 and ϵ_1) boundaries, respectively. By substituting Eq. (1) and Eq. (2) into Eq. (3), the SPR reflectivity can be simulated.

3. Results and discussion

3.1. Absorption spectrum of BOBzBT₂

Two peaks, at 450 nm and 481 nm, were observed using UV-VIS spectrophotometry. Interestingly, the double-peaked characteristic is similar to that of Rhodamine 6G, an organic material that has been used to demonstrate strong coupling [48–51]. Increasing the BOBzBT₂ concentration in the dilution, increases the absorbance as shown in Fig. 3(A). This is due to more light being absorbed as more BOBzBT₂ pentamers are present in the system. The double-peaked characteristic was also preserved, even with the addition of different creatinine solution. Referring to Fig. 3(B), by using 3BOBzBT₂:5CHCl₃ dilution, discernible quenching of the absorption spectrum is observed as the concentration of creatinine increases. This inverse Beer-Lambert Law is due to the gradual relaxation or inhibition of internal charge transfer between the sensing material and the analyte [52].

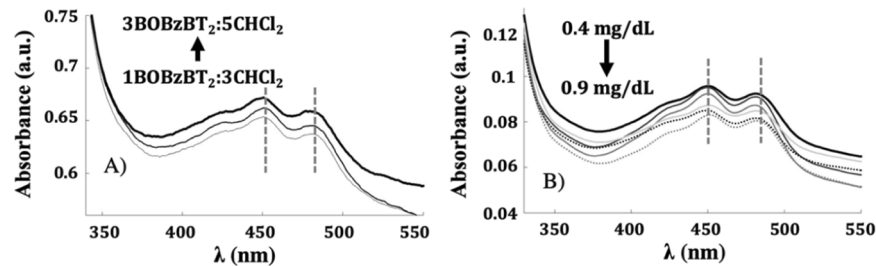


Fig. 3. The absorbance spectra for A) three BOBzBT₂: CHCl₃ dilutions and, B) 3BOBzBT₂: 5CHCl₃ dilutions with six concentrations of creatinine.

3.2. Strong coupling regime

With the dielectric layer sandwiched between a prism and a metal layer, the Otto configuration emulates the optical cavity. Consequently, the radiation leakage is significantly reduced [53]. An exciton-plasmon hybrid system can be formed when the energy-transfer rate between the exciton and the plasmon is larger than the rate of leakage in the system. This system has distinct eigenenergies and eigenstates when compared with the uncoupled system and can be represented by the Jaynes-Cumming model (Fig. 4(A)).

To investigate the existence of a strong coupling regime, SPR measurements using the unmodified, 1BOBzBT₂:3CHCl₃, the 1BOBzBT₂:2CHCl₃, and the 3BOBzBT₂:5CHCl₃ sensors were conducted. This is done by performing wavelength sweeping from 300 nm to 1000 nm at a fixed incident angle. The measurements were first obtained using a blank solution (0.0 mg/dL). As shown in Fig. 4(B), only a single dip, D1 at 453 nm (denoted by γ_p) is observed from the

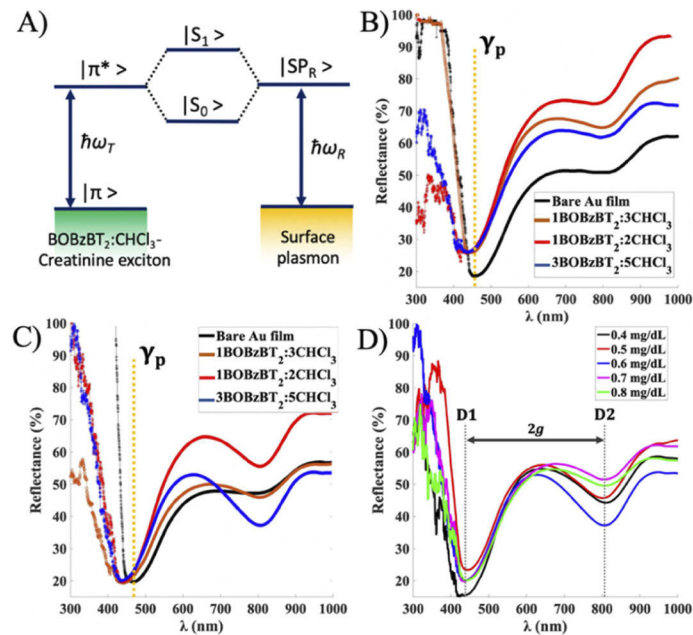


Fig. 4. A) The Jaynes-Cummings model of exciton-plasmon hybrid. SPR spectra obtained from unmodified sensor and BOBzBT₂-modified sensors using B) blank solution and C) 0.6 mg/dL concentration of creatinine solution. Gold dotted line represents the uncoupled plasmon resonance, γ_p . D) The left dip, D1 and the right dip, D2 from the reflectance spectra of the 3BOBzBT₂:5CHCl₃ modified sensor.

unmodified sensor. Using the 1BOBzBT₂:3CHCl₃-sensor, D1 shifted to the lower wavelength of approximately 447 nm.

By repeating the measurement with higher concentrations of BOBzBT₂, namely 1BOBzBT₂:2CHCl₃ and 3BOBzBT₂:5CHCl₃, D1 is shifted to approximately 435 nm. Besides that, a faint appearance of a right dip, D2 at a proximity of 800 nm, can be observed in the spectra obtained from modified sensors. The D1 wavelength obtained from the 1BOBzBT₂:3CHCl₃-sensor was shifted to 441 nm with the addition of 0.6 mg/dL creatinine solution, whereas both the 1BOBzBT₂:2CHCl₃ and 3BOBzBT₂:5CHCl₃ sensors maintained the similar D1 wavelength of approximately 435 nm (Fig. 4(C)). Moreover, the shifting of γ_p to approximately 467 nm is also observed. The D2 becomes more pronounced, especially in the spectra obtained from 1BOBzBT₂:2CHCl₃ and 3BOBzBT₂:5CHCl₃ sensors.

Two dips in the SPR measurement can be interpreted in two ways: either by the Long Range Surface Plasmon (LRSP) or by the strong coupling. Due to the use of a symmetric metal slab or film, LRSP is inherent in the Otto-SPR setup. Using this configuration, Otto was the first to observe the LRSP characteristic [54]. However, in LRSP setup, a thin metal film must be sandwiched by two dielectric layers with a similar RI. Given that the RI of the blank solution is 1.333 and the RI of the glass slide on which the Au film was deposited is 1.523, the resonance dip obtained from the unmodified sensor (represented by black line in Fig. 4 (B and C)) was the non-LRSP resonance dip obtained from the unmodified sensor. If the LRSP was caused by the introduction of BOBzBT₂:CHCl₃, the resonance dip should have a considerably narrower linewidth than a non-LRSP dip [55]. On the contrary, there was no discernible difference in the linewidth of the D1 obtained from the modified sensors and the unmodified sensor. Therefore,

it can be deduced that the two dips observed in the experiment may not have resulted from the LRSP.

The strong coupling occurs when the Rabi oscillation period is shorter than the damping time of both SP and the bare excitons [56]. To demonstrate that, the splitting width must be larger than the linewidth of the absorption line and the uncoupled plasmon line. Referring to Fig. 3, the linewidth of the absorption line is 0.56 eV with peak energies of 2.74 eV and 2.58 eV, respectively. On the other hand, the linewidths for γ_p were measured at 0.58 eV and 0.53 eV with resonance energies of 2.73 eV and 2.65 eV for the blank solution and 0.6 mg/dL creatinine solution, respectively. Meanwhile, the splitting width, $2g$ between D1 and D2 is approximately 1.24 eV (Fig. 4(D)), which is larger than the linewidths of the absorption and the uncoupled plasmon. This indicates that the strong coupling regime is achieved with splitting to damping ratio ($2g/\gamma_p$) of ~ 2.1 . Furthermore, the D1 and D2 were observed at resonance energies of 2.85 eV and 1.55 eV, respectively. These energies are the respective energies for the hybrid states $|S_1$ (the upper polariton) and $|S_0$ (the lower polariton) as depicted in Jaynes-Cumming model (Fig. 4(A)).

3.3. Strong coupling-induced resonance dip for sensing

The D2 in Fig. 4(D) resulted from the strong coupling regime and can be exploited for creatinine sensing applications. The corresponding D2 obtained at five different creatinine concentrations - for the bare Au, the 1BOBzBT₂:3CHCl₃-, 1BOBzBT₂:2CHCl₃- and the 3BOBzBT₂:5CHCl₃ respectively, is shown in Fig. 5. D2 is present at all BOBzBT₂ dilutions and at all creatinine concentrations. In contrast, by using the bare Au, D2 can only be observed when performing the SPR measurement using the creatinine solutions with a concentration of 0.7 and 0.8 mg/dL (see Fig. 5(A)). This is partly due to the increase in coupling efficiency between the excitons and surface plasmon due to more creatinine molecules being present in the solution.

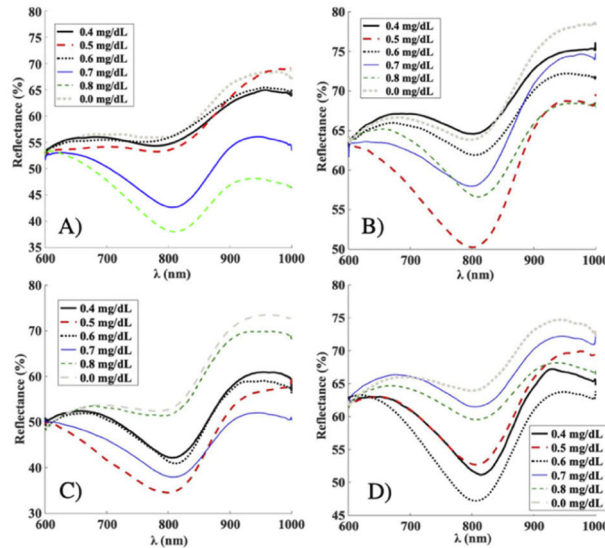


Fig. 5. The right dip, D2 for A) the unmodified sensor, B) the 1BOBzBT₂:3CHCl₃-Au sensor, C) the 1BOBzBT₂:2CHCl₃-Au sensor, and D) the 3BOBzBT₂:5CHCl₃-Au sensor.

Varying the creatinine concentrations shifts the resonance wavelength of D2. However, in the 1BOBzBT₂:3CHCl₃-sensor (Fig. 5(B)), a negative-shift was observed from 802.4 nm at a creatinine concentration of 0.4 mg/dL to 800.9 nm at 0.5 mg/dL before shifting to a larger value of 803.6 nm at 0.6 mg/dL. This was followed by another negative-shift to 797.6 nm at

0.7 mg/dL, before shifting to 809.9 nm at 0.8 mg/dL. The resonance shifting continues with the 1BOBzBT₂:3CHCl₃-sensor, as demonstrated in Fig. 5(C). By increasing the creatinine concentration from 0.4 mg/dL to 0.5 mg/dL, a negative-shift of $\Delta\lambda = 7.6$ nm is observed, and is followed by a positive-shift from 0.5 mg/dL to 0.7 mg/dL before a smaller resonance at a wavelength of 800 nm is obtained at 0.8 mg/dL.

The shift towards a lower wavelength or a negative-shift in an SPR sensor is not uncommon and was reported as early as the 1970s [57]. In a material-analyte matrix, the RI can also be influenced by the damping caused by a chemical reaction. Furthermore, the disproportionate association between the concentration of the analyte and the RI may account for the contribution of the tensorial components of the dielectric function. By using a higher concentration of BOBzBT₂ (i.e., 3BOBzBT₂: 5CHCl₃), the positive-shifting was observed with a creatinine concentration range of 0.4 mg/dL to 0.8 mg/dL (Fig. 5(D)). As compared to lower BOBzBT₂ concentrations, the demonstration of a monotonic relationship between creatinine concentration and the wavelength shift when using a higher concentration of BOBzBT₂ indicates the sensitivity of the BOBzBT₂ pentamer towards creatinine molecules.

In addition, there are two partial negative δ^- groups on the BOBzBT₂ pentamer, namely at an electron-rich atom such as S at the thiophene unit and O at the alkyloxy side chain. Meanwhile, the presence of NH and NH₂ groups on the creatinine molecule provides two partially positive polar groups, δ^+ . The polar interactions are likely to occur between the S atom and the NH group in the creatinine molecule, compared to another possible polar interaction of N-H...O. This is due to the fact that the red-shift in the N-H...S hydrogen-bond is almost twice as large compared with that for N-H...O [58]. Moreover, the binding energy of the N-H...S complex was also comparable to that of the indole-benzene complex.

3.4. Theoretical fitting with experimental results

The analysis was carried out by solving Eq. (3) at a fixed incident angle, α , following the experimental setup (Fig. 2(C)). The changes in the SPR response produced by varying the relative dielectric constant of the BOBzBT₂:CHCl₃-Creatinine layer, ϵ_2 are shown in Fig. 6(A). Increasing the value of dielectric constant, ϵ_2 leads to greater polarization of the medium. This induces attenuation on the accumulated charges in the vicinity of the resonance. As a result, the reduction of the net restoring force in the system shifts the resonance wavelength to a larger value. These conclusions are compatible with the experimental fact that the wavelength shifted as the RI changed, since the ϵ_2 is correlated to the RI.

The influence of the thickness of the spacer layer, d , on the SPR response is demonstrated in Fig. 6(B). When the gap is too large ($d \rightarrow \infty$), the magnitude of SP excitation has reduced - and therefore, the resonance will vanish. Moreover, at $d \rightarrow \infty$, the exciton is no longer localized - and the rate of light escape from the cavity is greater, resulting in reduced coupling efficiency. On the other hand, as the imaginary term of ϵ_2 increases, the resonance halfwidth is broadened, as shown in Fig. 6(C) - which is expected since the term itself is associated with the intrinsic losses of the system.

There was a robust agreement between the D2 observed experimentally and the response generated theoretically - in the vicinity of the resonance, as shown in Fig. 6(D). It was determined theoretically that to obtain a similar resonance wavelength to that in the experiment, the thickness of the BOBzBT₂:CHCl₃-creatinine layer should be approximately 130 nm. However, the curves deviated from each other at $\lambda \gg \lambda_{sp}$ and $\lambda \ll \lambda_{sp}$, respectively, which is mainly due to the limited ability of the theoretical model to predict the dynamics of the system at either larger or smaller wavelengths with respect to the resonance wavelength.

The fitting between the SPR curves obtained experimentally and in theory has enabled the values of the relative dielectric constant, ϵ_2 to be extracted - for 1BOBzBT₂: 3CHCl₃-creatinine, for 1BOBzBT₂:2 CHCl₃-creatinine and for 3BOBzBT₂:5 CHCl₃-creatinine. In the presence

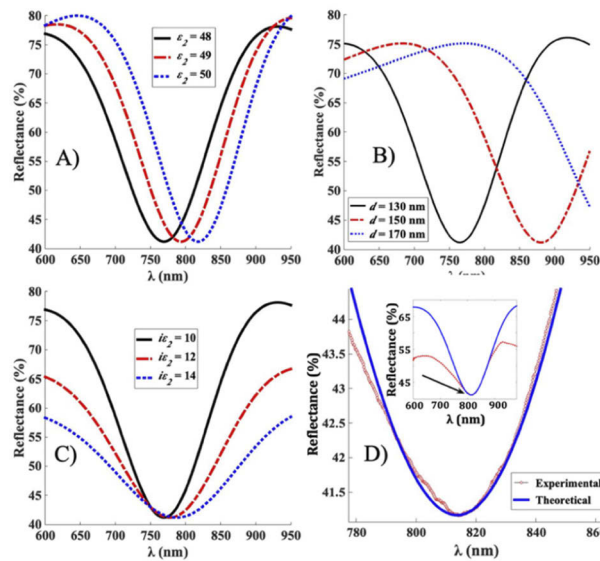


Fig. 6. The SPR spectra modelled using to Eq. (3) by varying A) ϵ_2 , B) d and C) $i\epsilon_2$. D) A good agreement between theoretical SPR reflectance spectra with the experimental spectra.

of BOBzBT₂ dilution, the dielectric constant, ϵ_2 fluctuated between approximately 49.2 and approximately 50. These values range between the dielectric constant values of dimethyl sulfoxide (DMSO) (CH₃)₂SO, another organosulfur compound, and hydrazine N₂H₄, at 20°C.

3.5. Sensor performance in quantifying creatinine in an aqueous solution

A typical SPR-based sensor utilizes the change in the local RI of the analyte near the metallic surface as a result of the direct interaction with the surface plasmon. The sensor's operating range was determined by measuring the relationship between analyte concentration and wavelength shift. In the present work, the addition of BOBzBT₂ pentamer to the system enables the formation of BOBzBT₂-creatinine complexes. The BOBzBT₂-creatinine excitons are then coupled with the surface plasmon to induce the strong coupling regime. As the concentration of creatinine varies, the energies of the hybrid states also vary, resulting in the shifting of the D1 and D2 resonance wavelengths.

However, as demonstrated in Fig. 7(A), by conducting the numerical analysis using Lumerical's FDTD software, it is demonstrated that D2 is more sensitive to the change in RI. The analysis was performed by varying the wavelength of the source light, oriented at an angle following the experimental setup. To simulate the excitons, 6 dipoles oriented at a 65° angle with respect to the horizontal axis were added between the BK7 prism and the Au film (inset of Fig. 7(A)). By changing the background RI, n , the variation of D2 is more pronounced compared to D1. Moreover, both the left and right peaks of D1 and D2 varied significantly.

The performance of the 3BOBzBT₂:5CHCl₃-sensor was investigated using different concentrations of creatinine solutions ranging from 0.4 to 0.9 mg/dL. By subtracting the D2 resonance wavelength obtained from the blank solution from the wavelength acquired at each creatinine concentration, the calibration plot is created. When measuring creatinine levels with creatinine solutions, the sensor showed a monotonically falling function (see Fig. 7(B)). On the contrary, none was observed when performing similar measurements using thiourea solutions with a concentration range of 0.4–0.9 mg/dL (inset Fig. 7(B)). Thiourea was chosen since it is typically present in the serum [59]. The finding further validates the sensor's selectivity for creatinine.

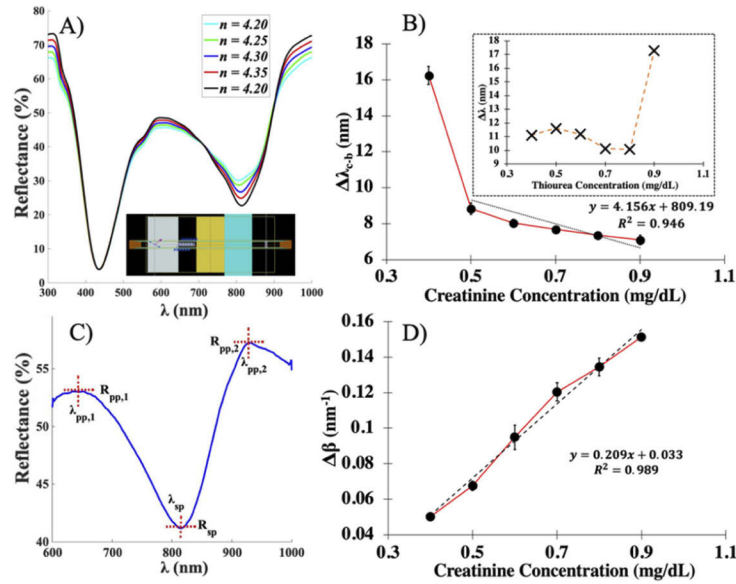


Fig. 7. A) The SPR spectra obtained using FDTD simulation. B) Experimental calibration plot ($N = 5$) of $3\text{BOBzBT}_2:5\text{CHCl}_3$ sensor. Inset shows the attempted calibration plot for thiourea solutions. C) The components of the SPR curve involve the derivation of Eq. (4). D) The improved calibration plot for the $3\text{BOBzBT}_2:5\text{CHCl}_3$ sensor.

Despite its promising trend, the wavelength variation between 0.4 mg/dL and 0.5 mg/dL is substantial. By excluding the response obtained from 0.4 mg/dL, the linear regression between 0.5 mg/dL and 0.9 mg/dL is constructed with a correlation coefficient of $R^2 = 0.946$. The sensor's sensitivity, which is determined by taking the slope of the response curve, is approximately evaluated at $4.156 \mu\text{L dL g}^{-1}$. The values of 0.32 mg/dL for the limit of detection (LOD) and 0.99 mg/dL for the limit of quantification (LOQ) were determined on the basis of the ICH guideline [60].

A normalisation procedure was proposed to improve the calibration curve obtained from the experimental result. This is done by utilizing left and right peaks that accompany D2 (peak $R_{pp,1}$ and peak $R_{pp,2}$ in Fig. 7(C)) and by plotting the difference between the proportionate coefficient, $\Delta\beta$ obtained from the blank solution following the creatinine concentrations. β is calculated by using the ratio between the difference in resonance depths and the wavelengths involving both $R_{pp,1}$ and $R_{pp,2}$ peaks namely;

$$\beta = \frac{\Delta R_1(\Delta R_2 - \Delta R_1)}{\Delta R_2} \Psi \quad (4)$$

where;

$$\Delta R_i = \left| \frac{R_{pp,i} - R_{sp}}{\lambda_{pp,i} - \lambda_{sp}} \right|, i = 1, 2 \quad (5)$$

Ψ is obtained by calculating the $\Delta R_2/\Delta R_1$ for the bare Au sensor in respect to the corresponding concentration of creatinine.

As demonstrated in Fig. 7(D)), the correlation coefficient, R^2 , is significantly improved compared with the experimental calibration curve (Fig. 7(A)). It shows that the detection range of the BOBzBT₂ modified sensor has been extended to 0.4 mg/dL. Following this formulation, the sensitivity of the sensor is valued at 0.209 dL mg^{-1} with a much lower detection limit (LOD) of 0.11 mg/dL. The LOQ was calculated at 0.36 mg/dL. The performance comparison between the experimental calibration curve and the modified calibration curve obtained by the formalism

of Eq. (4) is summarized in Table 1. The improvement was mainly contributed by the additional parameters to measure the D2. The utilization of SPR peaks also amplifies the faint wavelength shifting obtained from the direct experimental measurement.

In comparison with other works where, a non-strong coupling SPR sensor for creatinine sensing was utilized, the present work offers a lower detection range corresponding to the normal level of creatinine in serum. In [61], by using a commercially available SPR Navi 200 instrument and despite the addition of the creatininase enzymes, the obtained linear working range is 113.1 to 2261.9 mg/dL, which is beyond the range of normal creatinine concentration in serum. On the other hand, Arif et al. [62] proposed the SPR sensor chip that was modified with the artificial creatinine receptor to quantify the creatinine concentration. However, in spite of the complex sensor chip preparation, the linear working range is between 11.3 and 1130.9 mg/dL, which is inadequate to measure the creatinine concentration level in serum. With a much lower minimum working range of 0.4 mg/dL, the utilization of the strong coupling regime proposed in the present work has improved the sensitivity of the SPR-based sensor significantly without the need for the enzymes and complex preparation of the sensor.

Table 1. Comparison in terms of sensor performance between the experimental calibration curve and the theoretical calibration curve (Eq. (7)).

	Range (mg/dL)	LOD (mg/dL)	LOQ (mg/dL)	Sensitivity ^a	R ² (a.u.)
Experimental	0.4–0.9	0.32	0.99	415.6 nm L g ⁻¹	0.946 ^b
Theoretical (Eq. 4)	0.4–0.9	0.11	0.32	20.9 n L g ⁻¹ m ⁻¹	0.989

^aNote that the sensitivity obtained from the experimental calibration curve (Fig. 7(A)) and the theoretical calibration curve (Fig. 6(C)) are different due to the different Y-axis on the respective calibration curves.

^bWith the exclusion of 0.4 mg/dL.

As shown in Table 2, the proposed sensor is compared to reported sensors available in the literature in the following areas: technique, material used, linear range, sensitivity, and detection limit. In comparison to the previously proposed creatinine sensors, the presented strong coupling-based SPR has the advantages of being simple to use, relatively stable, good sensitivity, and inexpensive. Despite the higher LOD, the performance of the sensor is adequate for monitoring the normal range of creatinine in serum. Furthermore, as compared to the fabrication method used in this study, surface enhanced Raman scattering (SERS) and localized surface plasmon (LSPR) based sensors necessitate advanced ways to regulate the consistency of the fabricated sensor chip. As the present work aims to provide an alternative to the second step of the Jaffe method, i.e., monitoring the creatinine level in the PFF solution, exploiting the strong coupling in Otto-SPR configuration for sensor applications provides both simplicity and adequate performance.

Table 2. Comparison Comparison of the proposed sensor's performance to that of existing sensors.

Technique	Material used	Range (mg/dL)	LOD (mg/dL)	Ref.
SERS	Thiol-functionalized Ag films - Ag colloid	0.06 - 11.3	Not reported	[63]
LSPR	GO/AuNPs/MoS ₂ - NPs/CA	0 - 22.6	1.4	[64]
SERS/MOS	SPR/AgNPs/PPy film	0.1–11.3	0.002	[65]
Stamping SERS	PDMS/NPGDs with Ag-Au alloy	0.001 - 1.1	0.0001	[66]
Strong coupling based SPR	BOBzBT ₂ on Au film	0.4 - 0.9	0.11	Present work

4. Conclusions

We have reported a SPR-Otto creatinine sensor using a novel organic pentamer by exploiting the strong coupling between the excitons and surface plasmon. The combination of a large optical nonlinearity sensing material and a sandwiched material-analyte layer to simulate an optical cavity facilitates the formation of a strong coupling regime. The Au film sensor chip was immobilized with the organic pentamer 1,4-bis[2-(5-thiophene-2-yl)-1-benzothiophene]-2,5-dioctyloxybenzene (BOBzBT₂). The SPR measurement on different creatinine concentrations, a biomarker for CKD, was conducted using different concentrations of the BOBzBT₂ diluted in CHCl₃. The experimental results were investigated theoretically and show good agreement with the standard theoretical framework in the near-infrared region. The sensor with the highest BOBzBT₂ concentration demonstrates an operating range of 0.4–0.9 mg/dL. The experimental limit of detection (LOD) and limit of quantification (LOQ) of the sensor were determined to be 0.32 mg/dL and 0.99 mg/dL, respectively. The performance of the sensor was later improved to a LOD of 0.11 mg/dL and an LOQ of 0.36 mg/dL. This is accomplished by using a normalization of the calibration curve based on the strong coupling-induced dip. The setup's simplicity, along with good sensor performance due to the use of the strong coupling regime, should pave the way for the development of comparable sensors for a range of biomarkers.

Funding. Pusat Pengurusan Penyelidikan dan Instrumentasi (UKM-TR-016).

Disclosures. The authors declare no conflicts of interest.

Data availability. Data underlying the results presented in this paper are not publicly available at this time but may be obtained from the authors upon reasonable request.

References

1. V.S. Vaidya, M.A. Ferguson, and J.V. Bonventre, "Biomarkers of acute kidney injury," *Annu. Rev. Pharmacol. Toxicol.* **48**(1), 463–493 (2008).
2. J. Du, B. Zhu, W. R. Leow, S. Chen, T. C. Sum, X. Peng, and X. Chen, "Colorimetric detection of creatinine based on plasmonic nanoparticles via synergistic coordination chemistry," *Small* **11**(33), 4104–4110 (2015).
3. T. Küme, B. Sağlam, C. Ergon, and A. R. Sisman, "Evaluation and comparison of Abbott Jaffe and enzymatic creatinine methods: Could the old method meet the new requirements?" *J Clin Lab Anal* **32**(1), e22168 (2018).
4. Y. Zuo, Y. Yang, Z. Zhu, W. He, and Z. Aydin, "Determination of uric acid and creatinine in human urine using hydrophilic interaction chromatography," *Talanta* **83**(5), 1707–1710 (2011).
5. X. Luo, T. Qiu, W. Lu, and Z. Ni, "Plasmons in graphene: Recent progress and applications," *Mater. Sci. Eng., R* **74**(11), 351–376 (2013).
6. Y. Tang, X. Zeng, and J. Liang, "Surface plasmon resonance: An introduction to a surface spectroscopy technique," *J. Chem. Educ.* **87**(7), 742–746 (2010).
7. J. Homola, S. S. Yee, and G. Gauglitz, "Surface plasmon resonance sensors: Review," *Sens. Actuators, B* **54**(1–2), 3–15 (1999).
8. J. M. McDonnell, "Surface plasmon resonance: Towards an understanding of the mechanisms of biological molecular recognition," *Curr. Opin. Chem. Biol.* **5**(5), 572–577 (2001).
9. Y. Yuan, N. Yuan, D. Gong, and M. Yang, "A high-sensitivity and broad-range spr glucose sensor based on improved glucose sensitive membranes," *Photonic Sens.* **9**(4), 309–316 (2019).
10. W. Liu, Y. Shi, Z. Yi, C. Liu, F. Wang, X. Li, J. Lv, L. Yang, and P. K. Chu, "Surface plasmon resonance chemical sensor composed of a microstructured optical fiber for the detection of an ultra-wide refractive index range and gas-liquid pollutants," *Opt. Express* **29**(25), 40734–40747 (2021).
11. C. Ciminelli, M. Campanella, F. Dell'Olio, C. E. Campanella, and M. N. Armenise, "Label-free optical resonant sensors for biochemical applications," *Prog. Quantum Electron.* **37**(2), 51–107 (2013).
12. S. Pechprasarn, K. Ittipornnusun, T. Jungpanich, N. Pensupa, and N. Albut, "Surface plasmon biosensor platform for food industry," *Appl. Mech. Mater.* **891**, 103–108 (2019).
13. A. Shalabney and I. Abdulhalim, "Sensitivity-enhancement methods for surface plasmon sensors," *Laser. Photon. Rev.* **5**(4), 571–606 (2011).
14. E. Kretschmann and H. Raether, "Notizen: Radiative decay of non-radiative surface plasmons excited by light," *Zeitschrift Für Naturforschung A* **23**(12), 2135–2136 (1968).
15. D. Jang, G. Chae, and S. Shin, "Analysis of surface plasmon resonance curves with a novel sigmoid-asymmetric fitting algorithm," *Sensors* **15**(10), 25385–25398 (2015).
16. N. Kamaruddin, A. A. A. Bakar, N. Mobarak, M. S. Zan, and N. Arsad, "Binding affinity of a highly sensitive au/ag/au/chitosan-graphene oxide sensor based on direct detection of pb2+ and hg2+ ions," *Sensors* **17**(10), 2277 (2017).

17. T. M. Chinowsky and S. S. Yee, "Surface plasmon resonance sensing in capillaries," *Electron. Lett.* **35**(19), 1659 (1999).
18. A. Otto, "Excitation of nonradiative surface plasma waves in silver by the method of frustrated total reflection," *Z. Phys. A: Hadrons Nucl.* **216**(4), 398–410 (1968).
19. E. K. Akowuah, T. Gorman, and S. Haxha, "Design and optimization of a novel surface plasmon resonance biosensor based on Otto configuration," *Opt. Express* **17**(26), 23511 (2009).
20. P. Silva, A. Luna, C. Oliveira, S. C. Cavalcanti, G. O. Almeida Neto, M. A. de Santos, M. R. N. dos, I. Llamas-Garro, J.-M. Kim, G. Fernandes, and E. de Fontana, "Characterization of otto chips by particle swarm optimization," *J. Microwaves, Optoelectron. Electromagn. Appl.* **20**(1), 158–172 (2021).
21. Y. Lee, S. Sim, and J.-M. Kim, "Otto configuration based surface plasmon resonance with tunable air-gap using piezoactuator," *2019 International Conference on Optical MEMS and Nanophotonics (OMN)*, 64–65 (2019).
22. J. O. Maciel Neto, G. O. Cavalcanti, I. Llamas-Garro, J.-M. Kim, and E. Fontana, "Pressure sensing by surface plasmon resonance in the Otto configuration," *2016 IEEE SENSORS*, 1–3 (2016).
23. Y. Lee, J. Kim, S. Sim, I. Llamas-Garro, and J. Kim, "Air-gap interrogation of surface plasmon resonance in otto configuration," *Micromachines* **12**(8), 998 (2021).
24. E. Fontana, R. H. Pantell, and S. Strober, "Surface plasmon immunoassay," *Appl. Optics* **29**(31), 4694 (1990).
25. E. Bužavaitė-Vertelienė, V. Vertelis, and Z. Balevičius, "The experimental evidence of a strong coupling regime in the hybrid Tamm plasmon-surface plasmon polariton mode," *Nanophotonics* **10**(5), 1565–1571 (2021).
26. S. Dufferwiel, S. Schwarz, F. Withers, A. A. P. Trichet, F. Li, M. Sich, O. Del Pozo-Zamudio, C. Clark, A. Nalitov, D. D. Solnyshkov, G. Malpuech, K. S. Novoselov, J. M. Smith, M. S. Skolnick, D. N. Krizhanovskii, and A. I. Tartakovskii, "Exciton-polaritons in van der Waals heterostructures embedded in tunable microcavities," *Nat. Commun.* **6**(1), 8579 (2015).
27. A. R. Md Zain, N. P. Johnson, M. Sorel, and R. M. De La Rue, "Coupling strength control in photonic crystal/photonic wire multiple cavity devices," *Electron. Lett.* **45**(5), 283 (2009).
28. E. Cao, W. Lin, M. Sun, W. Liang, and Y. Song, "Exciton-plasmon coupling interactions: From principle to applications," *Nanophotonics* **7**(1), 145–167 (2018).
29. P. Törmä and W. L. Barnes, "Strong coupling between surface plasmon polaritons and emitters: A review," *Rep. Prog. Phys.* **78**(1), 013901 (2015).
30. Z. Balevičius, "Strong coupling between tamm and surface plasmons for advanced optical bio-sensing," *Coatings* **10**(12), 1187 (2020).
31. O. Pérez-González, J. Aizpurua, and N. Zabala, "Optical transport and sensing in plexcitonic nanocavities," *Opt. Express* **21**(13), 15847 (2013).
32. M. Wang, A. Krasnok, T. Zhang, L. Scarabelli, H. Liu, Z. Wu, L. M. Liz-Marzán, M. Terrones, A. Alù, and Y. Zheng, "Tunable fano resonance and plasmon-exciton coupling in single au nanotriangles on monolayer ws 2 at room temperature," *Adv. Mater.* **30**(22), 1705779 (2018).
33. J. Feist, J. Galego, and F. J. Garcia-Vidal, "Polaritonic chemistry with organic molecules," *ACS Photonics* **5**(1), 205–216 (2018).
34. C. Tserkezis, A. I. Fernández-Domínguez, P. A. D. Gonçalves, F. Todisco, J. D. Cox, K. Busch, N. Stenger, S. I. Bozhevolnyi, N. A. Mortensen, and C. Wolff, "On the applicability of quantum-optical concepts in strong-coupling nanophotonics," *Rep. Prog. Phys.* **83**(8), 082401 (2020).
35. R. M. Apetrei and P. Camurlu, "Review—functional platforms for (Bio)sensing: Thiophene-pyrrole hybrid polymers," *J. Electrochem. Soc.* **167**(3), 037557 (2020).
36. P. Norman, Y. Luo, and H. Ågren, "Structure-to-property relations for two-photon absorption of hydrocarbon oligomers," *Chem. Phys. Lett.* **296**(1-2), 8–18 (1998).
37. N. H. Azeman, M. A. A. Khushaini, R. Daik, A. G. Ismail, B. Y. Majlis, M. M. Salleh, T. H. T. A. Aziz, A. A. Bakar, A. R. M. Zain, and C. H. Teh, "Synthesis of a novel 1,4-bis[2-(5-thiophen-2-yl)-1-benzothiofene]-2,5-dioctyloxybenzene pentamer for creatinine detection," *Asian J. Org. Chem.* **10**(9), 202100374 (2021)..
38. P. Norman, P. Cronstrand, and J. Ericsson, "Theoretical study of linear and nonlinear absorption in platinum-organic compounds," *Chem. Phys.* **285**(2-3), 207–220 (2002).
39. E. Fontana, J.-M. Kim, I. Llamas-Garro, and G. O. Cavalcanti, "Microfabricated Otto chip device for surface plasmon resonance-based optical sensing," *Appl. Opt.* **54**(31), 9200 (2015).
40. T. Srivastava, A. Purkayastha, and R. Jha, "Graphene based surface plasmon resonance gas sensor for terahertz," *Opt. Quantum Electron.* **48**(6), 334 (2016).
41. L. Li, Y. Liang, J. Guang, W. Cui, X. Zhang, J.-F. Masson, and W. Peng, "Dual Kretschmann and Otto configuration fiber surface plasmon resonance biosensor," *Opt. Express* **25**(22), 26950 (2017).
42. A. N. Gortari, S. Bouchoule, E. Cambriil, A. Cattoni, L. Hauke, J. Enderlein, F. Rehfeldt, and A. Yacomotti, "Metasurface-based total internal reflection microscopy," *Biomed. Opt. Express* **11**(4), 1967 (2020).
43. A. Derkachova, K. Kolwas, and I. Demchenko, "Dielectric function for gold in plasmonics applications: Size dependence of plasmon resonance frequencies and damping rates for nanospheres," *Plasmonics* **11**(3), 941–951 (2016).
44. L. Nickelson, *Electromagnetic Theory and Plasmonics for Engineers* (Springer Singapore, 2019), (pp. 611–695).
45. S. Kawata, (Ed.). *Near-field optics and surface plasmon polaritons* (Springer, Berlin Heidelberg, 2001), (pp. 97–121).
46. P. B. Johnson and R. W. Christy, "Optical constants of the noble metals," *Phys. Rev. B* **6**(12), 4370–4379 (1972).

47. A.-B. M. A. Ibrahim, H. Eleuch, P. K. Choudhury, and M. K. Abd-Rahman, "Dielectric surface coated with thin partially-reflecting mirror – A revisit to Fresnel laws," *Optik* **207**, 164423 (2020).
48. T. K. Hakala, J. J. Toppari, A. Kuzyk, M. Pettersson, H. Tikkanen, H. Kunttu, and P. Törmä, "Vacuum rabi splitting and strong-coupling dynamics for surface-plasmon polaritons and rhodamine 6 g molecules," *Phys. Rev. Lett.* **103**(5), 053602 (2009).
49. Y. Fang, K. Blinn, X. Li, G. Weng, and M. Liu, "Strong coupling between Rhodamine 6G and localized surface plasmon resonance of immobile Ag nanoclusters fabricated by direct current sputtering," *Appl. Phys. Lett.* **102**(14), 143112 (2013).
50. S. R. K. Rodriguez and J. G. Rivas, "Surface lattice resonances strongly coupled to Rhodamine 6G excitons: Tuning the plasmon-exciton-polariton mass and composition," *Opt. Express* **21**(22), 27411 (2013).
51. N. I. Cade, T. Ritman-Meer, and D. Richards, "Strong coupling of localized plasmons and molecular excitons in nanostructured silver films," *Phys. Rev. B* **79**(24), 241404 (2009).
52. S. Ellairaja, K. Shenbagavalli, and V. S. Vasantha, "Ultrasensitive fluorescent biosensor for creatinine determination in human biofluids based on water soluble rhodamine b dye-au 3 + ions conjugate," *ChemistrySelect* **2**(3), 1025–1031 (2017).
53. A. R. Md Zain and R. M. De La Rue, "Control of coupling in 1D photonic crystal coupled-cavity nano-wire structures via hole diameter and position variation," *J. Opt.* **17**(12), 125007 (2015).
54. P. Berini, "Long-range surface plasmon polaritons," *Adv. Opt. Photonics* **1**(3), 484 (2009).
55. X. Zhao, X. Zhang, X.-S. Zhu, and Y.-W. Shi, "Long-range surface plasmon resonance sensor based on the GK570/Ag coated hollow fiber with an asymmetric layer structure," *Opt. Express* **27**(7), 9550 (2019).
56. Y. Huang, F. Wu, and L. Yu, "Rabi oscillation study of strong coupling in a plasmonic nanocavity," *New J. Phys.* **22**(6), 063053 (2020).
57. E. T. Arakawa, M. W. Williams, R. N. Hamm, and R. H. Ritchie, "Effect of damping on surface plasmon dispersion," *Phys. Rev. Lett.* **31**(18), 1127–1129 (1973).
58. H. S. Biswal and S. Wategaonkar, "Nature of the n-h...s hydrogen bond," *J. Phys. Chem. A* **113**(46), 12763–12773 (2009).
59. L. C. Chesley, "Observations on the absorption, apparent volume of distribution, and excretion of thiourea," *J. Clin. Invest.* **23**(5), 856–858 (1944).
60. "ICH Topic Q2 (R1) Validation of Analytical Procedures: Text and Methodology. Step 5: Note for guidance on validation of analytical procedures: text and methodology," European Medicines Agency (1995).
61. P.S. Menon, F. A. Said, G. S. Mei, D. D. Berhanuddin, A. A. Umar, S. Shaari, and B. Y. Majlis, "Urea and creatinine detection on nano-laminated gold thin film using Kretschmann-based surface plasmon resonance biosensor," *PLoS One* **13**(7), e0201228 (2018).
62. A. Arif Topçu, E. Özgür, F. Yılmaz, N. Bereli, and A. Denizli, "Real time monitoring and label free creatinine detection with artificial receptors," *Mater. Sci. Eng., B* **244**, 6–11 (2019).
63. Y. Lu, C. Wu, R. You, Y. Wu, H. Shen, L. Zhu, and S. Feng, "Superhydrophobic silver film as a SERS substrate for the detection of uric acid and creatinine," *Biomed. Opt. Express* **9**(10), 4988 (2018).
64. M. Li, R. Singh, C. Marques, B. Zhang, and S. Kumar, "2D material assisted SMF-MCF-MMF-SMF based LSPR sensor for creatinine detection," *Opt. Express* **29**(23), 38150 (2021).
65. C. Pothipor, C. Lertvachirapaiboon, K. Shinbo, K. Kato, K. Ounnunkad, and A. Baba, "Detection of creatinine using silver nanoparticles on a poly(Pyrrole) thin film-based surface plasmon resonance sensor," *Jpn. J. Appl. Phys.* **59**(SC), SCCA02 (2020).
66. M. Li, Y. Du, F. Zhao, J. Zeng, C. Mohan, and W.-C. Shih, "Reagent- and separation-free measurements of urine creatinine concentration using stamping surface enhanced Raman scattering (S-sers)," *Biomed. Opt. Express* **6**(3), 849 (2015).